

7/17/03

## **Control Systems of the Large Millimeter Telescope**

*Wodek Gawronski<sup>1</sup> and Kamal Souccar<sup>2</sup>*

<sup>1</sup>Wodek Gawronski  
Jet Propulsion Laboratory  
California Institute of Technology  
M.S. 238-528  
Pasadena, CA 91109  
Tel.: (818) 354-1783  
Fax: (818) 393-0207  
E-mail: [Wodek.K.Gawronski@jpl.nasa.gov](mailto:Wodek.K.Gawronski@jpl.nasa.gov)

<sup>2</sup>Kamal Souccar  
LMT Project, Astronomy Department  
University of Massachusetts  
LGRT 815  
Amherst, MA 01003  
Tel.: (413) 545-3443  
Fax: (413) 545-3192  
E-mail: [souccar@astro.umass.edu](mailto:souccar@astro.umass.edu)

## Abstract

The paper presents the analysis results (in terms of settling time, bandwidth, and servo error in wind disturbances) of four control systems designed for the Large Millimeter Telescope (LMT). The first system, called PP, consists of the proportional and integral (PI) controllers in the rate and position loops, and is widely used in the antenna and radiotelescope industry. The analysis shows that the PP control system performance is remarkably good when compared to similar control systems applied to typical antennas. This performance is achieved because the LMT structure is exceptionally rigid, however, it does not meet the stringent LMT pointing requirements. The second system, called PL, consists of the PI controller in the rate loop, and the Linear-Quadratic-Gaussian (LQG) controller in the position loop. This type of controller is implemented in the NASA Deep Space Network antennas, where pointing accuracy is twice that of PP control system. The third system, called LP, consists of the LQG controller in the rate loop, and the proportional-integral-derivative (PID) controller in the position loop. This type of loop has not been yet implemented at known antennas or radiotelescopes, but the analysis shows that its pointing accuracy is the ten times better than PP control system. The fourth system, called LL, consists of the LQG controller in both the rate loop, and the position loop. It is the best of the four, with accuracy 250 better than the PP system, thus is worth further investigations, to identify implementation challenges for the telescopes of high pointing requirements.

## 1. Introduction

The Large Millimeter Telescope (LMT) Project is the joint effort of the University of Massachusetts at Amherst and the Instituto Nacional de Astrofísica, Óptica, y Electrónica (INAOE) in Mexico. The LMT is a 50m diameter millimeter-wave radio-telescope, see Fig.1, designed for principal operation at wavelengths between 1mm and 4mm. The telescope is being built atop Sierra Negra (4640m), a volcanic peak in the state of Puebla, Mexico. Site construction and fabrication of most of the major antenna parts is underway, with telescope construction expected to be complete in 2005.

The LMT will be a significant step forward in antenna design since, in order to reach its pointing and surface accuracy specifications, it must outperform every other telescope in its frequency range. The largest existing telescope with surface error superior to the LMT is the 15m James Clerk Maxwell Telescope, located at the summit of Mauna Kea (4092m) in Hawaii, and there is no telescope of any size, which reaches the LMT pointing requirements. The antenna designer expects that this system will point the telescope to its specified accuracy of 1 arcsec under conditions of low winds and stable temperatures. However, under the maximum operating wind conditions, the pointing will degrade to a few arcseconds (rms). The pointing challenges and their solutions are discussed in Refs. [1] and [8].

It is known [2] that the LQG (Linear Quadratic Gaussian) controllers guarantee wide bandwidth and good wind disturbance rejection properties, thus they are used for the antennas with stringent pointing requirements in the presence of wind disturbances. For antennas and radiotelescopes the LQG control systems can be implemented in two different ways: at the telescope rate-loop or at the position loop. The paper analyzes and compares the performance of the LQG controllers used in both loops. The analysis is augmented with the performance of the PI (Proportional and Integral) controller. The latter analysis is available for the comparison purposes (PI controller is a standard antenna industry feature), since the implementation of the LQG controller requires preliminary installation of PI controllers in both rate and position loops. The implementation of the LQG algorithm needs an accurate telescope model, which can be obtained from field tests of the telescope. Therefore a telescope must be operational before the LQG controller implementation.

Why do we need an accurate rate-loop model? It can be explained as follows. The performance of a controller improves with the gain increase. However, high gains excite structural vibrations in the telescope. For a PI controller structural vibrations cannot be easily controlled since the structural deformations are not directly measured by encoders. The LQG controller uses a Kalman filter to estimate telescope vibrations, overcoming the difficulty of direct measurement. The Kalman filter consists of an analytical model of the telescope that needs to be accurate to produce accurate estimate of the telescope structural dynamics.

The control system of the LMT consists of rate and position loop, as shown in Fig.2. Four control systems will be analyzed. They have the following structure

- **PP** control system, with **PI** controller in the position loop, and **PI** controller in the rate loop,
- **PL** control system, where the **PI** controller is in the rate loop, and **LQG** controller is in the position loop.
- **LP** control system, where the **LQG** controller is in the rate loop, and **PID** controller is in the position loop
- **LL** control system, where the **LQG** controller is in the rate loop, and **LQG** controller is in the position loop.

The configurations of the control systems are presented in Table1. The PP control system is a typical telescope control system configuration. The PL case is the configuration of the NASA Deep Space Network (DSN) antenna control system that was implemented at the 34-meter antennas in Goldstone, CA, and which has been considered by MAN Technologie [1], [8]. The LP and LL control systems have not yet been implemented.

The paper presents the performance analysis (in terms of bandwidth, step responses, and wind disturbance rejection properties) of the four control systems as applied to the LMT. This analysis shall help to evaluate and select the control system, not only for the LMT, but also for other antennas and radiotelescopes of a similar design.

## 2. The PP Control system

The PP control system consists of the PI controller in the position loop, and PI controller in the rate loop. Its Simulink model is shown in Fig.3a, and the rate-loop subsystem in Fig.3b. The controller is shown in Fig.3c, assuming that  $k_f = 0$ . In this design the position-loop PI controller is complemented with the feedforward (FF) loop to improve the tracking properties, especially at high rates, and with a command preprocessor (CPP) to avoid large overshoots during target acquisition and to avoid limit cycling during slewing.

### 2.1. The Rate-Loop Model

The rate-loop model is shown in Fig.3b. It consists of the finite element model of the telescope structure (marked “Discrete Time FEM”), which includes the drives, and azimuth and elevation rate loop controllers. It is a discrete-time (digital) control system, with 0.001s sampling time. The proportional and integral gains of the azimuth controller are 300, and for the elevation controller proportional gain is also 300, and the integral gain is 400. The bandwidth of the rate-loop transfer function is 1.0 Hz, both in azimuth, and in elevation.

## 2.2. Command Preprocessor

Before the position loop is presented we consider the rate and acceleration limits imposed at the drives. The acceleration limits prevent motors from overheating (the motor current is proportional to telescope acceleration). During tracking the telescope motion is within the rate and acceleration limits. However, during slewing, the large position offset commands exceed the acceleration limit, or both acceleration and rate limits. When limits are exceeded the telescope dynamics are no longer linear, and the telescope becomes unstable, which is observed in the form of limit cycling (periodical motion of constant magnitude and of low frequency). Since the limit cycling is caused by commands that exceed the acceleration and rate limits, one can easily avoid the instability by properly shaping commands, such that the limits are not exceeded.

The command preprocessor (CPP) modifies the telescope commands such that they remain unaltered if they do not exceed the rate and acceleration limits, and processes the command to the maximum acceleration and rate limits if the limits are exceeded by the command. The block diagram of CPP is shown in Fig.4. The CPP algorithm represents an integrator, rate and acceleration limits, variable-gain controller, and a feedforward gain. Its input is a command  $r$ , and its output is the modified command  $r_f$ .

The variable gain  $k$  depends on the CPP tracking error  $e$ :

$$k(e) = k_o + k_v e^{-\beta|e|}$$

where  $e = r - r_f$ . For the LMT we selected the following parameters:  $k_o = 0.3$ ,  $k_v = 1.0$ , and  $\beta = 20$  for both azimuth and elevation. The plot of the gain  $k$  vs. error  $e$  is shown in Fig.5. More on CPP, see [3].

Figure 6 shows how the CPP transforms 10 deg step command for the LMT. The transformed step command shows the initial rise at the maximal acceleration, followed by maximal rate slope, and deceleration slowdown (which is smaller than the maximal deceleration in order to avoid excessive telescope shaking). By processing the commands the CPP allows for smooth telescope responses to step offsets and eliminate telescope limit cycling during slewing, see the following section on the position loop analysis.

### 2.3. Feedforward Loop

The feedforward loop is added to improve its tracking accuracy, especially at high rates. The feedforward loop differentiates the command, and forwards it to the rate-loop input, see Fig.3a. The derivative is the inversion the rate loop transfer function. In this way we obtain the open-loop transfer function from the command to the encoder approximately equal to 1. Indeed, the magnitude of the rate-loop transfer function  $G_r$  is shown in Fig.7. It can be approximated (up to 1 Hz) with an integrator ( $G_{rapprox} = \frac{1}{s}$ ), which is shown in the same figure, dashed line. The feedforward transfer function is a derivative ( $G_{ff}(s) = s$ ) shown in Fig.7, dash-dotted line, so that the overall open-loop transfer function is a series of the feedforward and the rate loop  $G_o(s) = G_r(s)G_{ff}(s)$ , which is approximately equal to 1 up to the frequency 1 Hz. In this way, the transfer function of the system is equal 1 (up to 1 Hz) without applying position feedback. The position feedback is added to compensate disturbances and system imperfections.

### 2.4. Position Loop

The position loop model is shown in Fig.3. It consists of the rate loop model, PI and feedforward controllers in azimuth and elevation, command preprocessors in azimuth and elevation, and rate and acceleration limiters in azimuth and elevation. The telescope rate limit is 1.0 deg/s, and the acceleration limit is 0.5 deg/s<sup>2</sup>, both in azimuth and elevation.

The PI controller gains were selected to minimize settling time and servo error in wind gusts. They also guarantee zero steady state error for constant rate tracking. The proportional gain is 3.0, and the integral gain is 1.0.

The position-loop transfer functions for azimuth and elevation are shown in Fig.8. It follows from this figure that the azimuth bandwidth is 1.2 Hz, while the elevation bandwidth is 1.8 Hz (the bandwidth is the frequency for which the magnitude of the transfer function falls below level 0.7). Note that the position-loop bandwidth is higher than the rate loop bandwidth, both in azimuth and elevation. Note also that the elevation axis bandwidth is higher than the azimuth axis bandwidth, mainly because elevation transfer function has few resonances, and that the resonances are well damped. Azimuth bandwidth is lower since the controller gains are low in order to prevent excitation of multiple resonances.

In order to evaluate settling time we simulated its step responses for small (0.01 deg), and for large (3.0 deg) steps. The azimuth step responses are shown in Fig.9, for the telescope with and without CPP. From the plots one can see that there is no overshoot when CPP was implemented, and that the settling time is 3.0 s (small steps) in azimuth and elevation. Without CPP we observe overshoots for small steps, and the settling time 4.5 s in azimuth and elevation. For larger steps (e.g. when slewing) the telescope becomes unstable (showing limit cycling), see Fig.9.

The wind gusts time history was obtained from the wind spectrum, see Ref. [4]. The plots of the servo error in azimuth and elevation are shown in Fig.10, in black color.

The PP control system analysis showed also that LMT is a sturdy structure. Its fundamental frequency is 1.7 Hz (compared to a typical radiotelescope, which nominally are 1.3 Hz, as shown in Fig.11). The rigid structure allows for high controller gains (3.0 proportional gain and 1.0 integral gain). For comparison, the NASA Deep Space Network antenna fundamental frequency is 1.8 Hz (although, as a smaller structure it should have higher frequency), and allows for 0.5 proportional gain, and for 0.1 integral gain (3.0 proportional gain and 1.0 integral gain destabilize it). Higher gains mean wider bandwidth (over 1 Hz), faster response (settling time 3 s), and improved wind disturbance rejection properties. In conclusion, the LMT performs better than it could be expected for the PP type control system.

### 3. The PL Control system

The PL control system consists of the LQG controller in the position loop, and PI controller in the rate loop.

#### 3.1. Rate Loop

In this case the rate-loop model of telescope is as in Fig.3a. It consists of the structure and drive model, and azimuth and elevation rate loop controllers (PI type). The PI gains of the rate controllers were given in Section 2.1.

#### 3.2. Position Loop

The position loop is presented in Fig.3, where the PI controllers are replaced with the LQG controllers, as in Fig.3c. It consists of the same rate-loop model as PP control system, the LQG controller with feedforward loop, command preprocessor, and rate and acceleration limits. The CPP parameters are as follows:  $k_v = 6$ ,  $k_o = 0.6$ , and  $\beta = 20$ , for azimuth and elevation.

The LQG controller structure is shown in Fig.12. The controller includes the estimator, which is an analytical model of the telescope. The estimator is driven by the same input ( $u_c$ ) as the telescope, and also by the estimation error  $\varepsilon$  (the difference between the actual rate  $y$  and the estimated rate  $y_{est}$ ). The error is amplified with the estimator gain  $k_e$  to correct for transient dynamics. The estimator output are the estimated telescope states that consist of the telescope rate and the telescope flexible deformations  $x_f$ . The latter are the missing vibration measurements, which allow for suppression of the telescope vibrations. The gains of the rate-loop LQG controller were obtained from the LQG design procedure, see Refs. [5], [6], [7] and [9].

We evaluated the performance of the PL control system using settling time, bandwidth, and servo error in wind gusts. The step responses for small (0.01 deg) and large (3 deg) steps are shown in Fig.13a,b. Figure 13a shows 1.6 s settling time in azimuth, 1.2 s settling time in elevation, 18% overshoot in azimuth, and 35% overshoot

in elevation. The position loop transfer functions for azimuth and elevation are shown in Fig.14. They show wide bandwidth of 1.3 Hz in azimuth and 1.5 Hz in elevation.

The wind gusts simulations show 0.15 mdeg rms servo error in azimuth and 0.74 mdeg rms servo error in elevation, as shown in gray on the servo error plot of Fig.10. These numbers are compared with the PP control system (0.35 mdeg in azimuth and 1.4 mdeg in elevation). This means that the LQG controller improves the servo error in wind over the PID controller by factor 2.3 in azimuth, and by factor 1.9 in elevation.

The obtained results on the LQG position controller are promising. The telescope settling time of 1.6 s, bandwidth 1.3 Hz, wind servo error 0.76 mdeg, or 2 times smaller than from the PP control system.

## **4. The LP Control system**

The LP control system consists of the PID (Proportional, Integral, and Derivative) controller in the position loop, and LQG controller in the rate loop. Its Simulink model is shown in Fig.3a, and the rate-loop subsystem in Fig.3b.

### **4.1. Rate Loop**

The Simulink model of the open-loop telescope is shown in Fig.3b, with the rate feedback removed. The open-loop model is scaled to obtain maximal rate of 1 deg/s for 10 V command (a standard input to motor drives). For this open-loop model we designed an LQG controller, and evaluated the performance of the rate-loop LQG controller by using step responses and transfer functions of azimuth and elevation. The settling time is 0.2 s in azimuth and elevation and the bandwidth is 1.6 Hz and 1.8 Hz in azimuth and elevation, respectively.

### **4.2. Position Loop**

The position loop is as in Fig.3, where the azimuth and elevation rate controller are now of the LQG type. Besides the rate-loop, it consists of the PID controller with feedforward loop, the command preprocessor, and rate and acceleration limiters. The feedforward loop forwards the command rate to the rate-loop input. The following PID gains were selected: proportional gain 10, integral gain 6, and derivative gain 5, for both

azimuth and elevation. The CPP parameters are as follows:  $k_v = 6$ ,  $k_o = 0.93$ , and  $\beta = 30$ , for azimuth and elevation.

The position loop performance was evaluated using step responses, bandwidth, steady-state errors due to rate offsets, and servo errors in wind gusts. The step responses for small (0.01 deg) and large (3 deg) steps are shown in Fig.15, showing 0.6 s settling time and no overshoot for both azimuth and elevation.

The position loop transfer functions for azimuth and elevation are shown in Fig.16. They show wide bandwidth of 200 Hz in azimuth and 20 Hz in elevation. The steady state errors due to rate offsets are zero.

The wind gusts simulations to 12 m/s wind are plotted in white on Fig.10. The figure shows 0.012 mdeg rms servo error in azimuth and 0.150 mdeg rms servo error in elevation. These small numbers show that the LQG controller in the rate loop improves the servo error in wind over the PP control system by factor 30 in azimuth, and by factor 10 in elevation.

The obtained results on the LQG rate controller are very promising. The telescope performance exceeds the expectation, since its settling time is 0.6 s, the bandwidth is 10 Hz, wind servo error is 0.15 mdeg, or 10 times smaller than from the PID controller.

## 5. The LL Control system

Finally, we designed the telescope control system with the LQG controller in the rate and position loop. This novel configuration in the antenna industry is possible now, due to availability of digital drives that replace analog ones. However, LQG loops lack the simplicity of PID loops – their tuning is complex. More experience is required to draw conclusions about LL controllers maintenance and performance issues.

The rate loop of the LL system is identical as for the LP control system. The position loop controller was designed to minimize the servo error in the wind gusts. The position loop characteristics are plotted in Figures 17 and 18. From Fig.17 it follows that the system settling time is 0.5 s, and there is no overshoot, both in azimuth and elevation. From Fig.18 one can find that the bandwidth is 20 Hz in azimuth and 40 Hz in elevation. Finally, the wind gusts simulations to 12 m/s wind are plotted in the zoomed insert in Fig.10. The figure shows 0.0012 mdeg rms servo error in azimuth and 0.0057 mdeg rms

servo error in elevation, which gives the total rms error of 0.0058 mdeg. It is 250 times smaller than the error of the PP control system. Thus the LL control system performance is the best of all presented system, although the system is the most complicated and will require careful tuning of both rate and position loop LQG controllers in order to obtain the predicted performance.

## 6. Conclusions

This paper presented the LMT control systems and evaluates its performance, which is summarized in Table 2. Based on the performed analysis we conclude that:

- The PP control system, widely used in the antenna and radiotelescope industry, shows improved pointing accuracy when compared to similar control systems applied to typical antennas or telescopes. It was achieved because the analysis showed the exceptionally rigid LMT structure.
- The PL control system, implemented at the NASA Deep Space Network antennas, has twice better pointing precision in wind than PP system.
- The analysis shows that pointing accuracy in wind of the LP control system is ten times better than PP system. This significant reduction was achieved because of the expanded bandwidth of the rate loop. It has not been yet implemented at known antennas or radiotelescopes.
- The analysis shows that its pointing accuracy in wind of the LL control system is 250 times better than PP system. The LL system has not been yet implemented at known antennas or radiotelescopes.

Finally, some comments on the obtained performance estimates of the telescope are necessary. The estimates, the best currently available, include some unknown factors. First, the presented telescope performance is based on the analytical models the structure and the drives, which do not represent an accurate dynamics of the telescope. To improve the accuracy a model shall be derived from the system identification and data collected at the real telescope. Next, the wind disturbance torques are applied to the drives, while in reality the wind acts on the entire structure, including the dish surface. Finally, the RF beam movement, the ultimate goal of the control, is not directly measured. Instead

azimuth and elevation encoders are used, which only partially reflected the beam position. The encoders – although relatively precise – cannot exactly measure the actual beam position due to their distant location from the beam focal point, which is the RF beam location.

The performed analysis shows the impact of the telescope controllers on its pointing accuracy, and should help to select the most effective system (in terms of cost and precision). Both LP and LL control systems are worth further investigations in hope that its implementation will meet the stringent pointing requirements.

### **Acknowledgement**

This work was partially funded from the National Science Foundation under grant AST-0100793, and the Advance Research Project Agency, Sensor Technology Office, DARPA Order No. C134 Program Code No. 63226E, issued by DARPA/CMO under contract MDA972-95-C-0004.

### **References**

1. P. Eisentraeger, and M. Suess, "Verification of the Active Deformation Compensation System of the LMT/GMT by End-to-End Simulations," in: *Radio Telescopes*, Proceedings of SPIE, Vol.4015, 2000.
2. W. Gawronski, "Antenna Control Systems: From PI to  $H_{\infty}$ ," *IEEE Antennas and Propagation Magazine*, vol.43, no.1, 2001.
3. W. Gawronski, W. Almassy, "Command Pre-Processor for Radiotelescopes and Microwave Antennas," *IEEE Antennas and Propagation Magazine*, vol.44, No2, 2002
4. W. Gawronski, "Three Models of Wind-Gust Disturbances for the Analysis of Antenna Pointing Accuracy," *IPN Progress Report 42-149*, January-March 2002, pp. 1-15, May 15, 2002. [http://ipnpr.jpl.nasa.gov/tmo/progress\\_report/42-149/149A.pdf](http://ipnpr.jpl.nasa.gov/tmo/progress_report/42-149/149A.pdf)

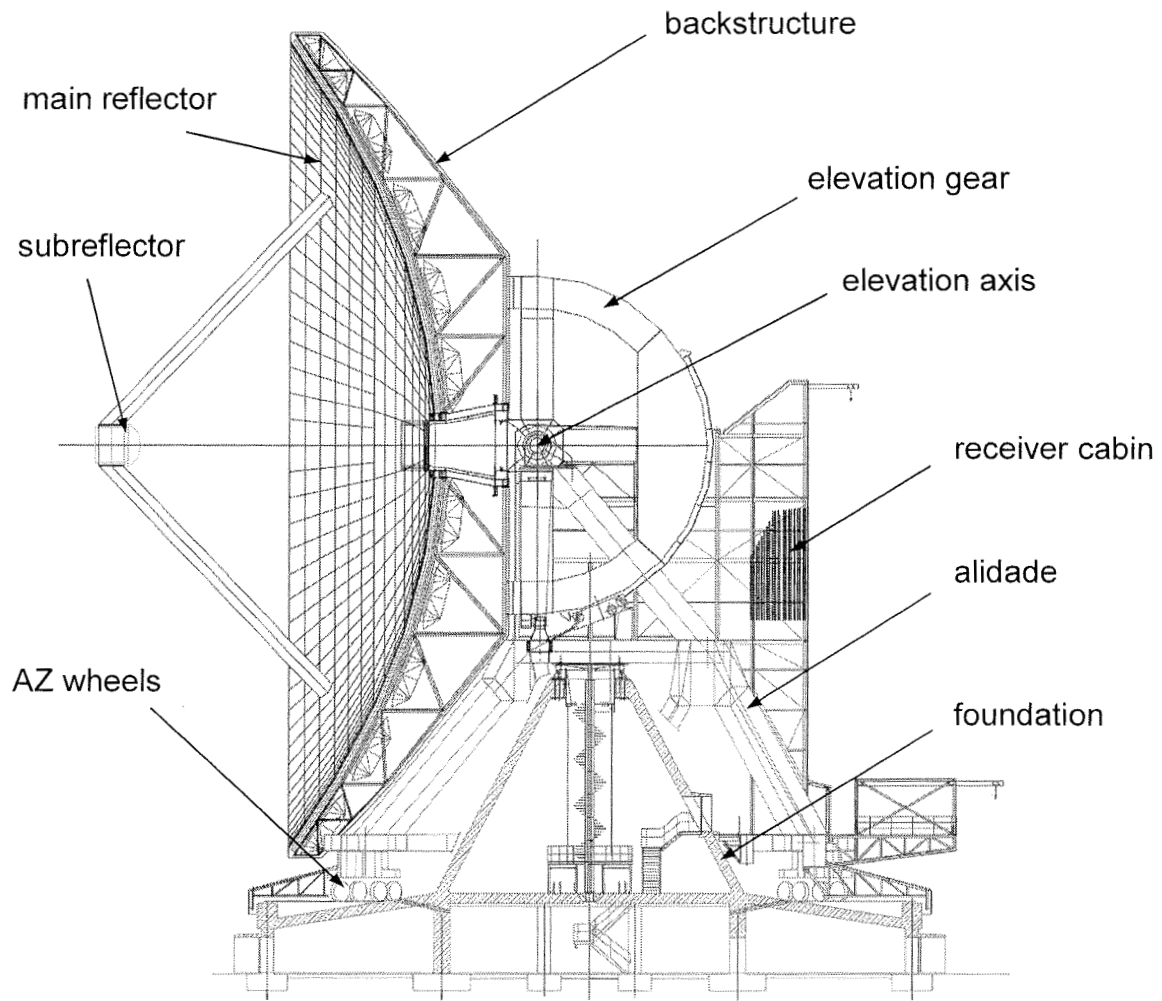
5. Gawronski, W., Racho, C., Mellstrom, J., "Application of the LQG and Feedforward Controllers for the DSN Antennas," *IEEE Trans. on Control Systems Technology*, vol.3, 1995.
6. Gawronski, W., "Design of a Linear Quadratic Controller for the Deep Space Network Antennas," *AIAA Journal of Guidance, Control, and Dynamics*, vol.17, 1994.
7. W. Gawronski, *Dynamics and Control of Structures*, Springer, 1998.
8. H.J. Kaercher, and J.W.M. Baars "The Design of the Large Millimeter Telescope/Gran Telescopio Milimetrico (LMT/GTM)," in: *Radio Telescopes*, Proceedings of SPIE, Vol.4015, 2000.
9. Maneri, E., and W. Gawronski, "LQG Controller Design Using GUI: Application to Antennas and Radio-Telescopes," *ISA Transactions*, 2000, vol. 39, No.2, pp.243-264.

**Table 1.** Configurations of the control systems of the Large Millimeter Telescope

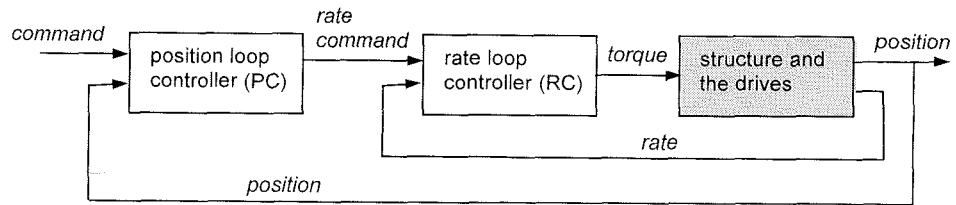
LMT control system	Rate loop controller	Position loop controller
PP	PI	PI
PL	PI	LQG
LP	LQG	PID
LL	LQG	LQG

**Table 2.** Performance of the PP, LP, PL and LL control systems

Control system	Settling time s	Overshoot %	Bandwidth Hz	Wind gust servo error mdeg
PP	3.0	20	1.2	1.48
LP	0.6	0	20	0.15
PL	1.4	20	1.4	0.76
LL	0.5	0	20	0.004

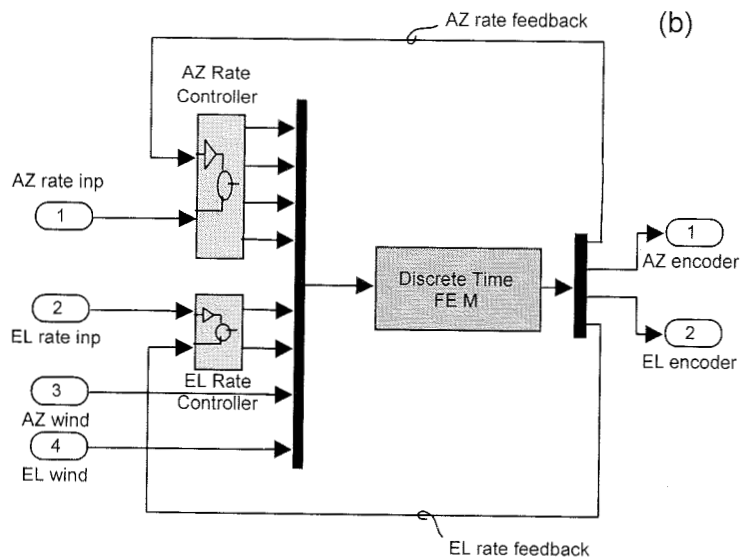
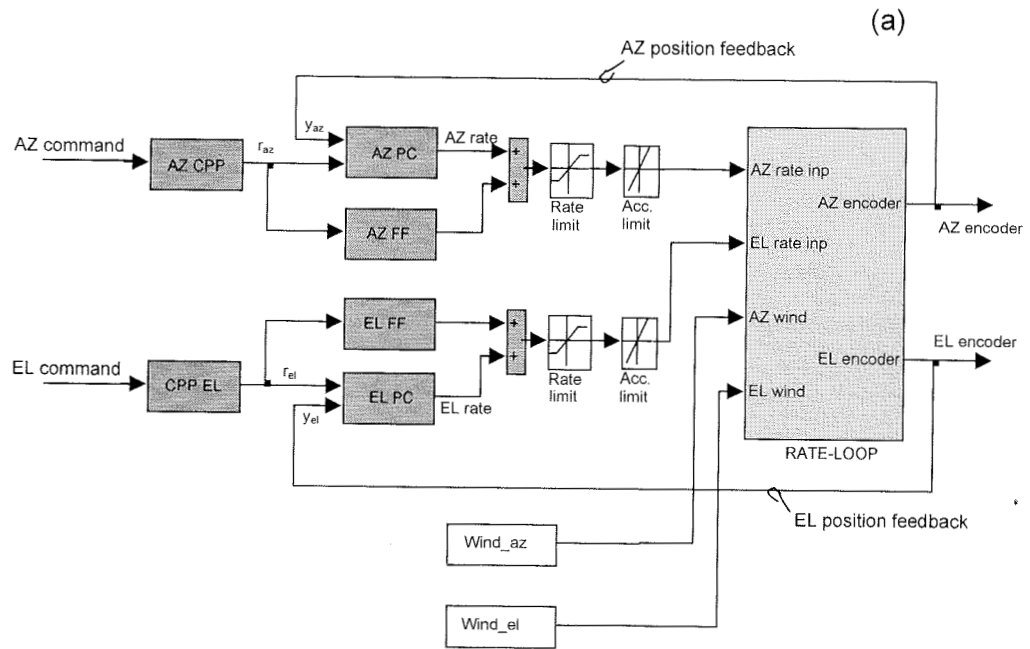


**Figure 1.** A drawing of the Large Millimeter Telescope. The whole telescope structure rotates with respect to vertical axis (azimuth) on azimuth wheels, and the dish rotates with respect to horizontal (elevation) axis.



**Figure 2.** Four control systems of the LMT:

- (1) PP control system, where  $RC=PI$ , and  $PC=PI$ ,
- (2) PL control system, where  $RC=PI$ , and  $PC=LQG$ ,
- (3) LP control system, where  $RC=LQG$ , and  $PC=PID$ , and
- (4) LL control system, where  $RC=LQG$ , and  $PC=LQG$ .



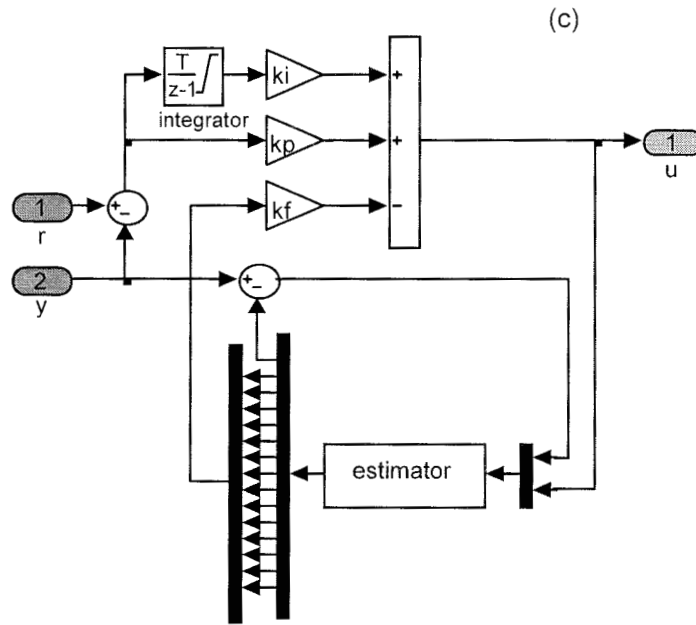


**Figure 3.** The Simulink model of (a) the position loop, and (b) the rate loop system, and (c) the controller (for  $k_f = 0$  it is a PI controller, for  $k_f \neq 0$  it is an LQG controller)

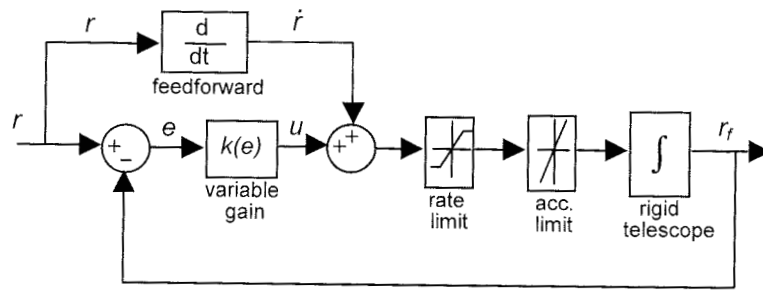


**Figure 4.** CPP block diagram

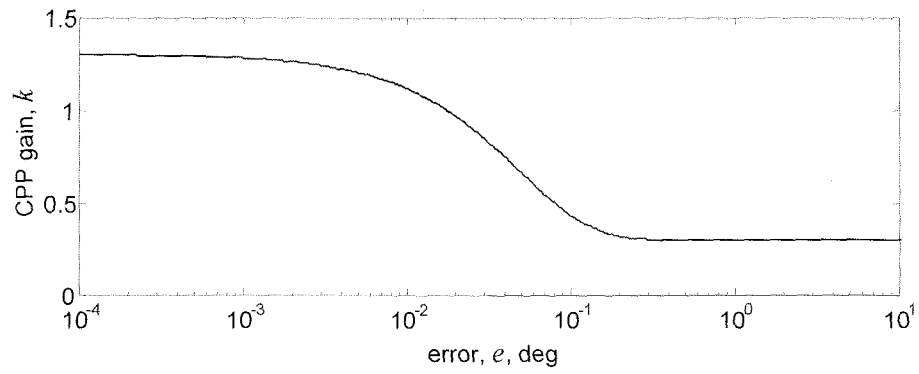


**Figure 5.** CPP gain  $k$  versus CPP error  $e$ .

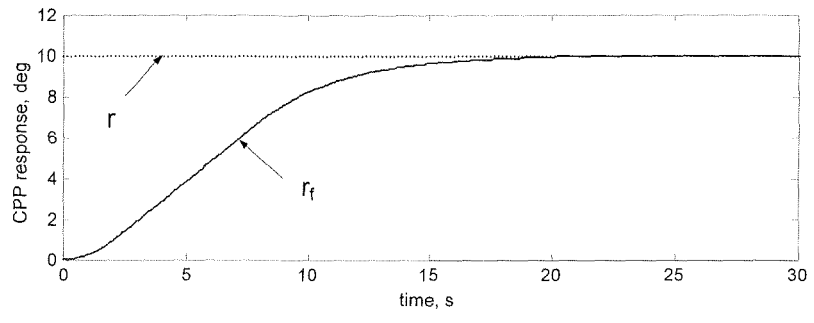


**Figure 6.** CPP response ( $r_f$ ) to 10 deg step command ( $r$ ).

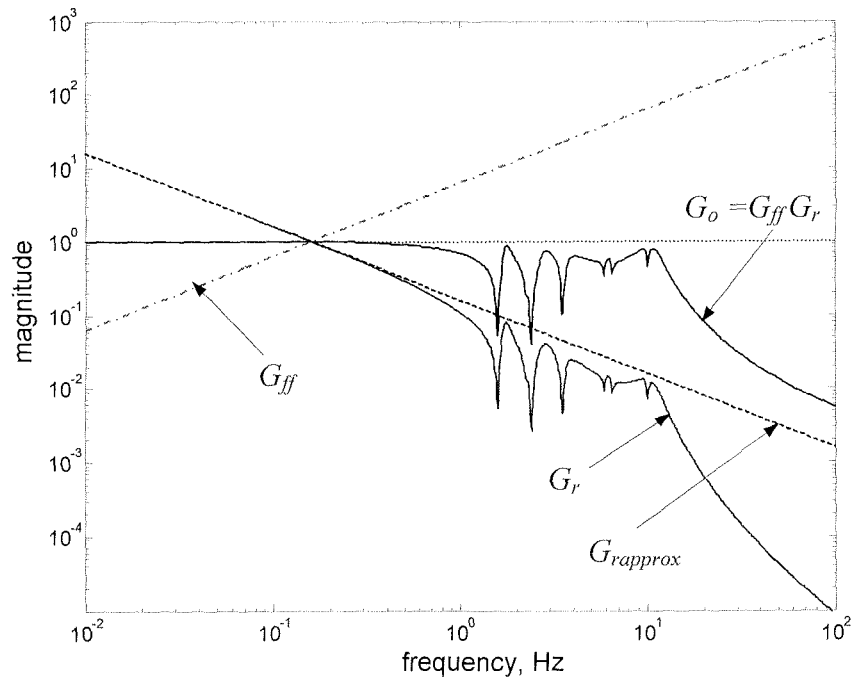


**Figure 7.** The feedforward action illustrated by the magnitudes of the transfer functions ( $G_r$  is the rate-loop transfer function,  $G_{rapprox}$  is the rate-loop transfer function approximation,  $G_{ff}$  is the feedforward loop transfer function, and  $G_o = G_{ff} G_r$  is the transfer function of the series connection of feedforward and rate-loops).

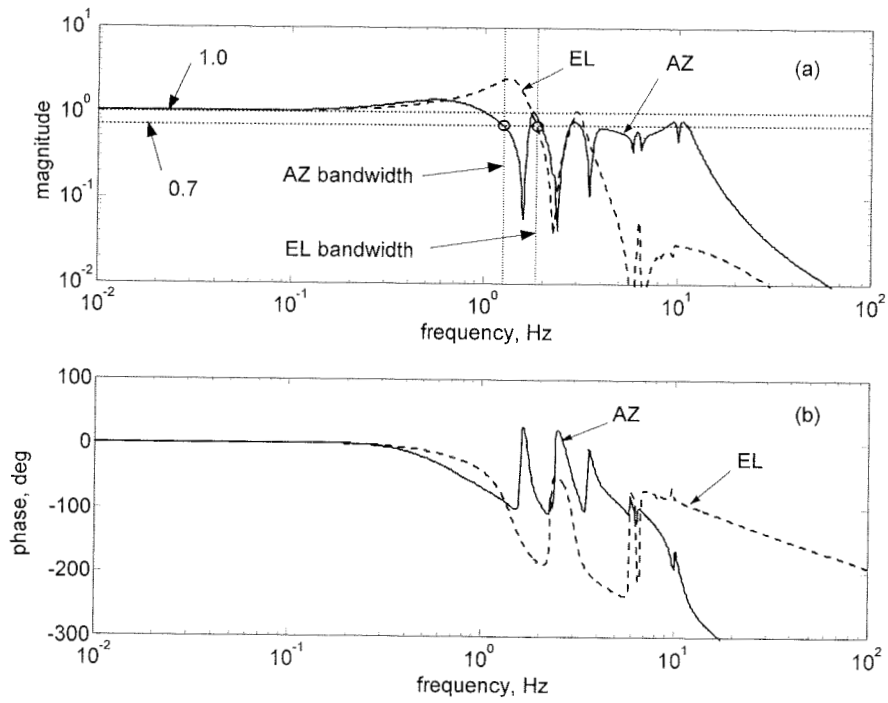


**Figure 8.** Position-loop transfer function in azimuth (solid line), and in elevation (dashed line): (a) magnitude, and (b) phase.

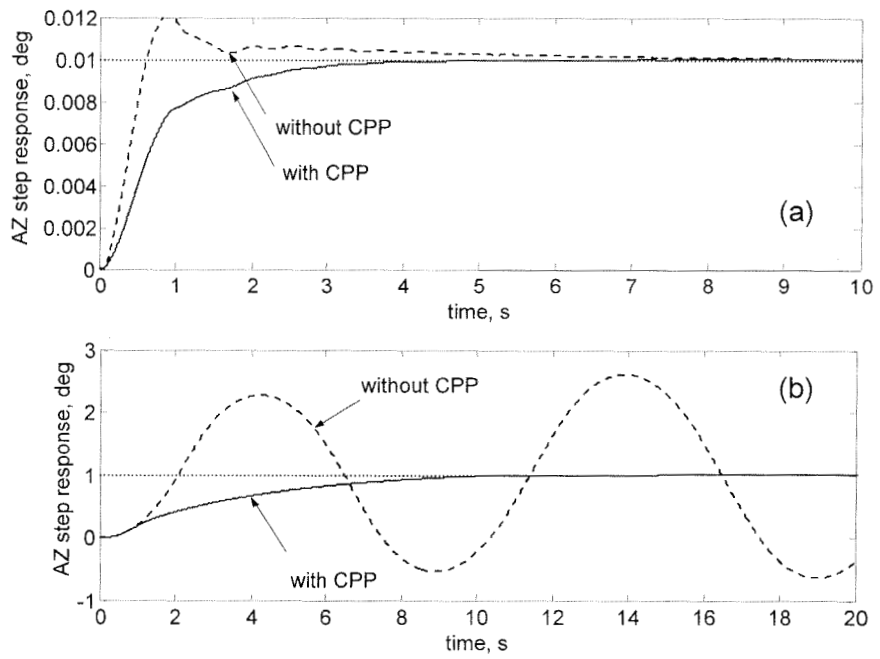


**Figure 9.** Telescope responses in azimuth, with CPP (solid line) and without CPP (dashed line): (a) to 0.01 deg step, and (b) to 1 deg step.

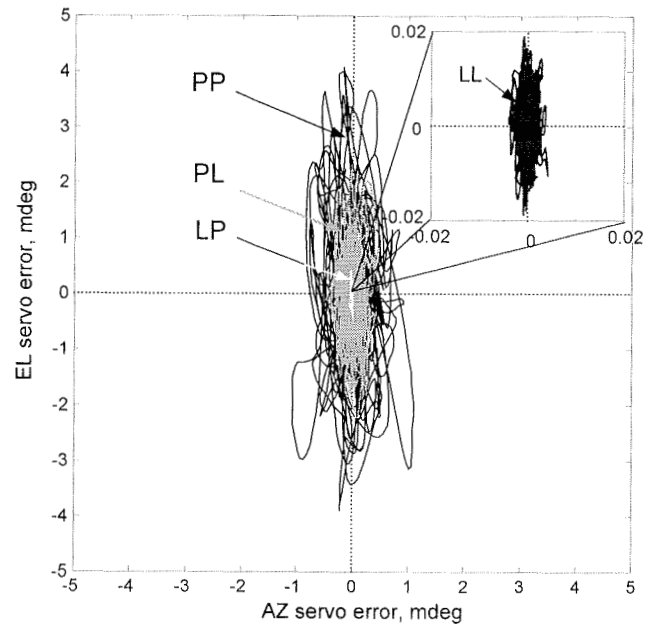


**Figure 10.** Telescope servo error in 12 m/s wind gusts: with PP control system (black), with PL control system (gray), with LP control system (white), and with LL control system (zoomed insert).

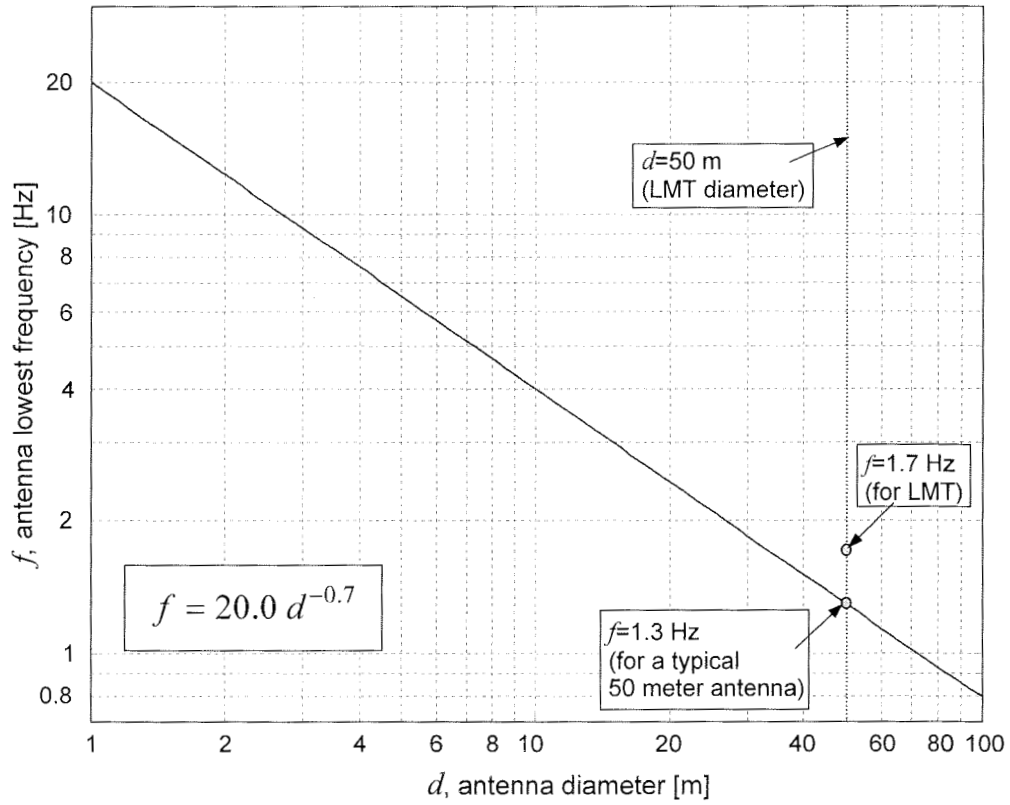


**Figure 11.** Antenna fundamental frequency (Hz) vs. antenna diameter (m). This plot is based on data from the Lowest Servo Resonant Frequency Chart by the Aerospace Corporation

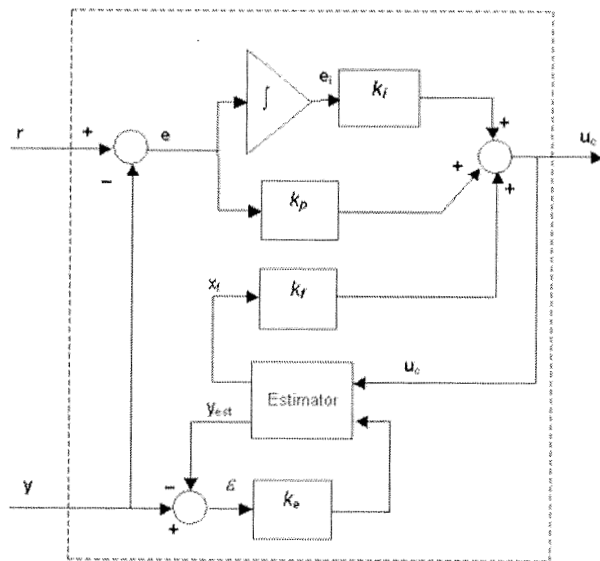


**Figure 12.** The LQG controller structure

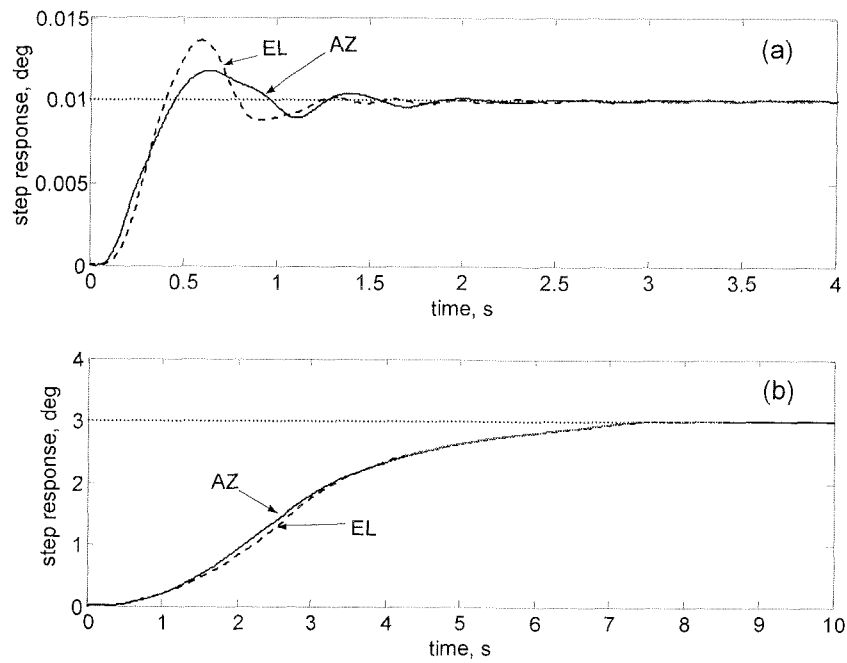


**Figure 13.** The PL control system responses to (a) 0.01 deg step, and (b) 3 deg step

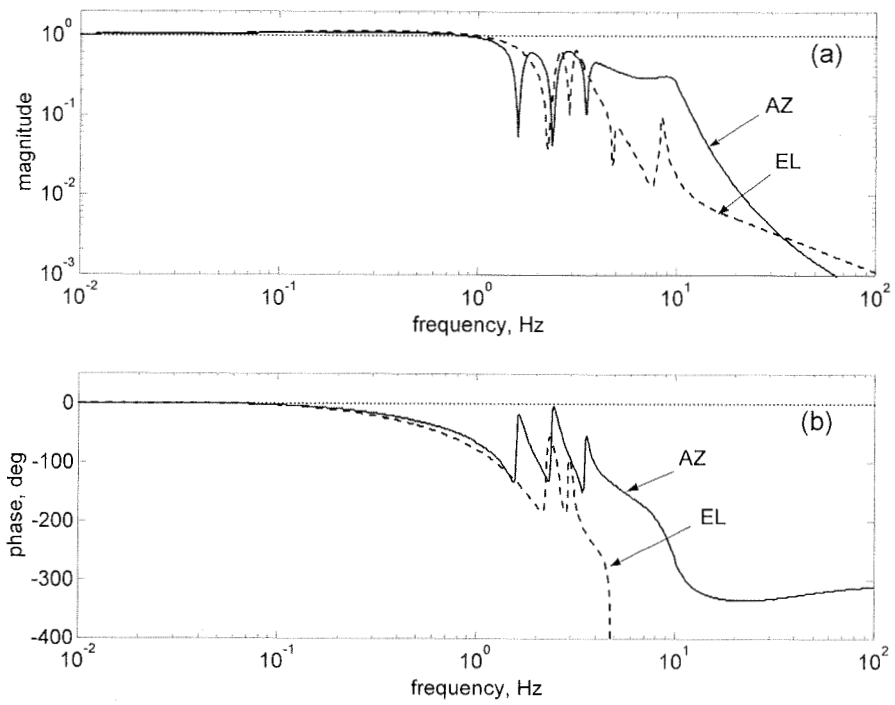


**Figure 14.** Azimuth and elevation transfer functions of the PL control system: (a) magnitudes, and (b) phases

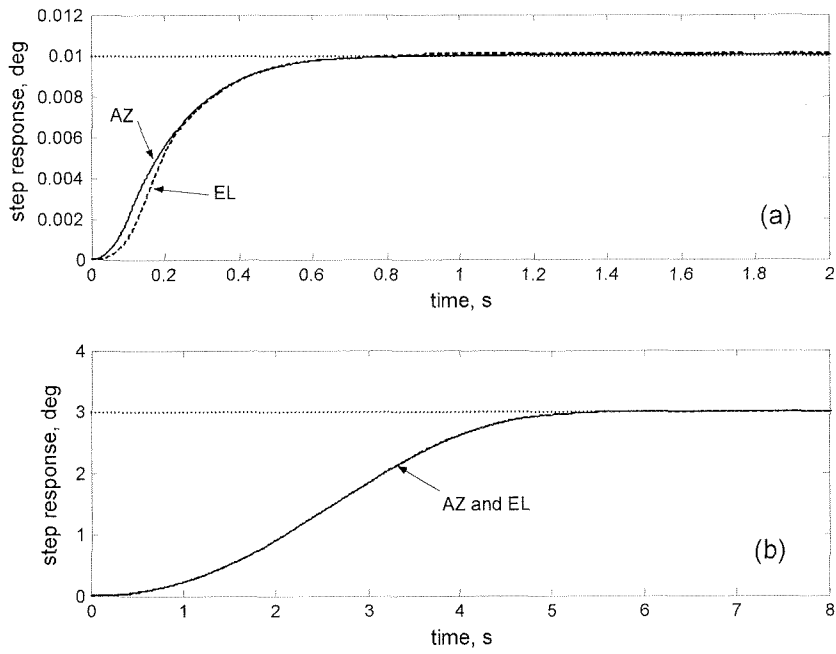


**Figure 15.** The LP control system position loop response to (a) 0.01 deg step, and (b) 3 deg step.

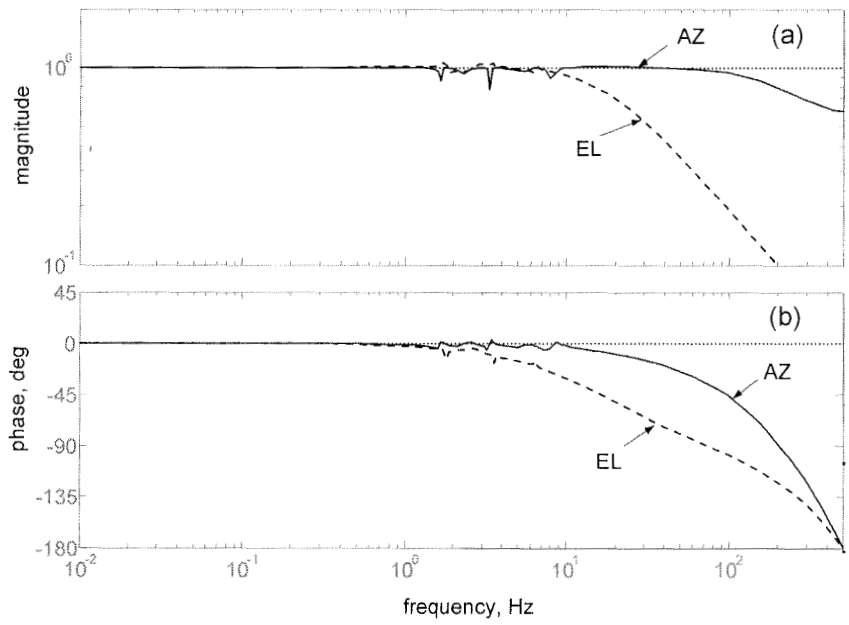


**Figure 16.** Azimuth and elevation position loop transfer functions of the LP control system: (a) magnitudes and (b) phases

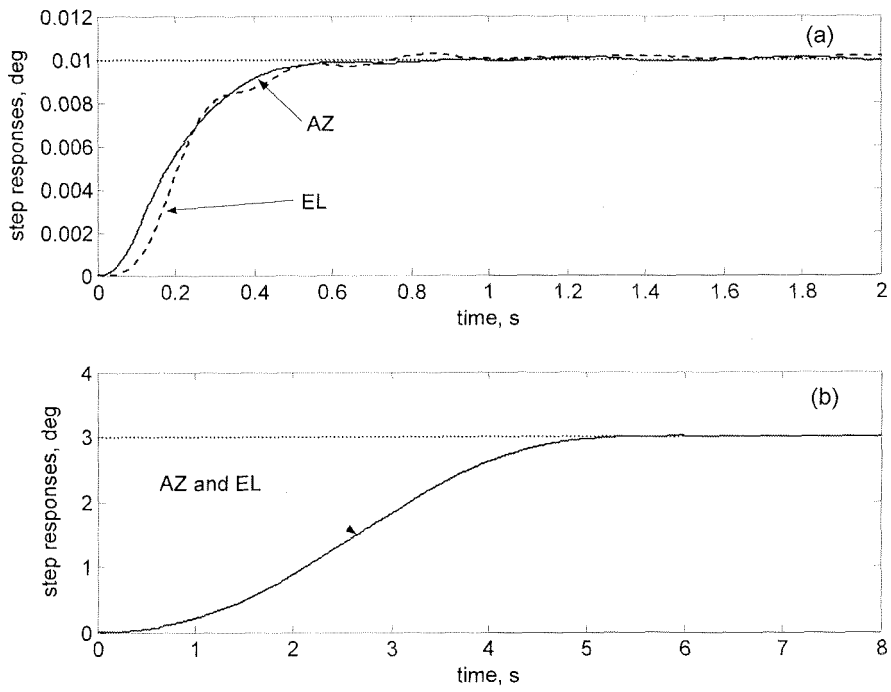


**Figure 17.** The LL control system position loop response to (a) 0.01 deg step, and (b) 3 deg step.

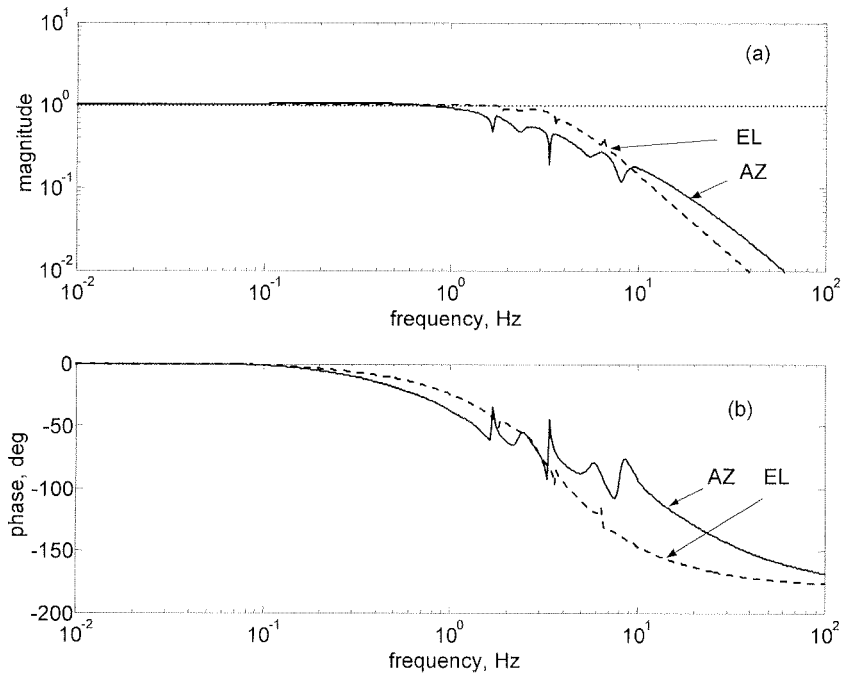


**Figure 18.** Azimuth and elevation position loop transfer functions of the LL control system: (a) magnitudes and (b) phases